DOI: 10.13009/EUCASS2019-651



# Design aspects and characterisation of a resonance igniter for oxygen/methane in-orbit propulsion systems

*Paul Lungu, Christian Bauer and Oskar J. Haidn*
*Technische Universität München, Institute for Turbomachinery and Flight Propulsion*
*Boltzmannstraße 15, 85748 Garching, Germany*
*paul.lungu@ltf.mw.tum.de, christian.bauer@ltf.mw.tum.de, oskar.haidn@ltf.mw.tum.de*

## Abstract

In this document the present studies on an oxygen/methane resonance ignition system are displayed. The work focuses on experimentally identifying and categorizing the main driving parameters of resonant heating performance. High frequency pressure data is used to identify acoustic characteristics of the resonance system. Based on this dataset, an optimized system design is elaborated. The results of preliminary ignition tests are outlined and the ability of said system to produce an ignition is demonstrated.

## 1. Introduction

In the context of EU REACH regulations, hydrazine and derivatives like MMH will become listed as materials of very high concern in the near future [1], among others due to their toxic and carcinogenic properties [2]. As a result, handling efforts and costs for these propellants, currently the most common used by spacecraft, will substantially increase [3]. This, in turn, increases the viability of other propellant combinations as a replacement. LOX and LCH4 are of particular interest since they are both non-toxic and yield a specific impulse about 10% higher than MMH/NTO. Furthermore, compared to LH2 for example, their higher boiling points allow propellant storage with zero boil-off [4, 5].
However, LOX/LCH4 lacks the hypergolic properties of MMH/NTO, making an ignition system necessary. For in-orbit mission profiles, e.g. debris removal, where a multitude of engine re-ignitions are required, a resonance ignition system offers multiple advantages. Besides a potentially unlimited lifetime, the passive working principle of this igniter type offers possible low hardware mass and high system reliability [6, 7].
The overall project which is the context of this document aims at the design, testing and optimisation of a resonance igniter for in-orbit propulsion, also considering aspects of the propellant feed system and engine operation. Here, design characteristics, resonant heating optimisations and an ignition capability evaluation are presented for a new small scale igniter prototype.

## 2. Fundamentals

The basic requirement of a resonance igniter is the capability of heating gas by acoustic modes. This state can be generated by directing an under-expanded free jet from a nozzle towards a cavity, with the Mach disk in proximity of the cavity inlet, as shown in Figure 1, [6].

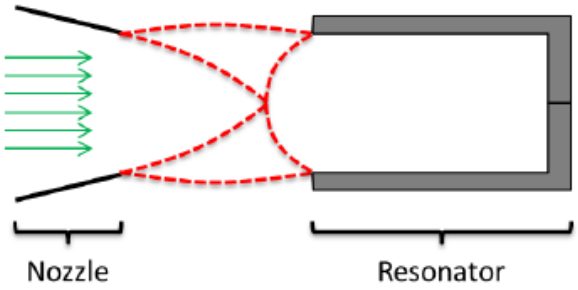


Figure 1: Nozzle-resonator configuration [6]

DOI: 10.13009/EUCASS2019-651



The occurrence of the heating effect depends, among others, on nozzle pressure and nozzle-resonator distance and is accompanied by distinct high-frequency pressure oscillations [8], with a system of shockwaves periodically travelling up and down the resonator cavity. By repeated compression of a gas portion near the closed end of the resonator, the gas is heated over time due to irreversible effects [9]. The temperatures reached at the closed end can exceed the stagnation temperature of the gas by far [10].
The operation and heating performance of a resonator configuration depends on a number of factors. Aside of the aforementioned nozzle pressure and nozzle-resonator distance, resonator and nozzle geometries and gas properties (e.g. heat capacity and molar mass) are driving parameters. The substantial influence of the gas type upon resonant heating performance is depicted in Figure 2, [11].

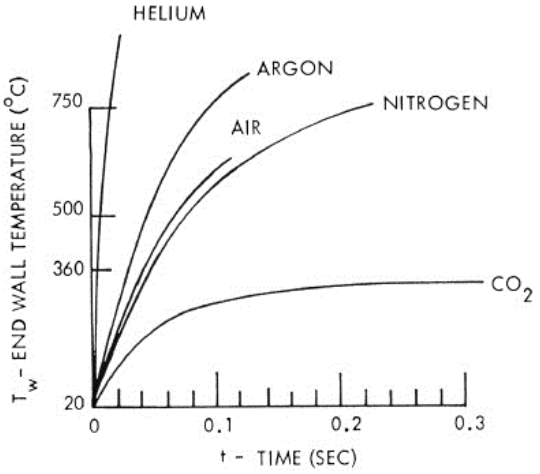


Figure 2: Resonant heating performance for a variety of gases [11]

For experimental and numerical investigations, two non-dimensional parameters are of particular importance. The first is the s/d ratio or s/d, defined as the nozzle-resonator distance s divided by the nozzle exit diameter d. The second is the nozzle pressure ratio or NPR, defined in **(1)**.

$$NPR = \frac{p_n}{p_e} \quad \textbf{(1)}$$

Here $p_n$ is the nozzle inlet pressure which equals the free jet total pressure assuming isentropic expansion and $p_e$ is the static pressure downstream of the nozzle exit surrounding the free jet.
It was shown by Sarohia and Back that for a resonator configuration several distinct modes of oscillations and hereby accompanied heating mechanisms exist [12]. For the application presented here the jet regurgitant mode (JRM) and the jet screech mode (JSM) are of particular interest.
The jet regurgitant mode is characterized by an inflow and outflow phase of the resonator with the distance from the nozzle to the free jet shock structure smaller than the nozzle-resonator-distance. During the inflow phase, compression waves travel towards the closed end of the cavity, and are reflected back to the inlet. Subsequently, expansion waves form at the inlet and propagate into the cavity, causing outward flow of gas and collision of the nozzle jet flow. These expansion waves reflect at the closed end of the cavity and travel back towards the inlet, the outward flow from the tube weakens and the free jet shock structure forms again at the resonator inlet. This point marks the transition to the inflow phase and the completion of the JRM cycle, which operates near the resonance cavity fundamental frequency [12].
The jet screech mode is triggered when the nozzle-shock structure distance is equal or higher than the nozzle-resonator-distance. A shock forms at the inlet of the resonance cavity and oscillates at high frequencies which are varying with s/d and NPR [12].

## 3. Preceding developments

In the past a substantial variety of resonance igniter designs has been successfully tested for various propellant combinations like hydrogen/oxygen [13, 14], and kerosene/oxygen [15], to name only a few examples. However to date none of these designs were used as actual flight hardware. One possible reason might be that the s/d for optimum resonant heating performance shifts depending on NPR, and thus, in many designs on inlet nozzle pressure.
In order to mitigate this issue, studies were performed where it was shown that the range of s/d for effective resonant heating can be extended by particular designs of inlet nozzle geometries [16, 17]. A coaxial nozzle with such a

DOI: 10.13009/EUCASS2019-651



geometrical design is implemented in the Z1 igniter, for which design and initial tests are outlined by Bauer in [18], where this system is designated as 'Configuration 2'.
Another method which eliminates the dependency of optimum s/d to inlet pressure is to ensure choked flow in the outlet nozzle of the igniter chamber in any mode of operation, thus keeping the NPR constant despite inlet pressure variations. Based on this the operating point of the same hardware Z1 was shifted to higher inlet pressures to allow outlet nozzle choking for the test campaign described in [7].

## 4. Ignition system design

The design of the new ignition system, in the following designated as 'Z2', is based to a great extent on the preceding Z1 design but on a smaller scale, suitable for a rocket engine in the 500 N thrust range. An overview of the Z2 configuration is given in Figure 3. Igniter operation is initiated by introducing oxygen into the inlet nozzle (2) to generate a free jet directed into the resonator cavity (3) where resonant heating of the oxygen occurs. This will be referred to as pre-heating. Subsequently, methane is added into the nozzle flow by the CH4 injector (1) and the inlet nozzle drives a combustible mixture to the heated area inside the resonator, triggering ignition. Following this, the combustion zone extends out of the resonator and the ignition chamber produces a hot gas torch which critically expands through the outlet nozzle (4).

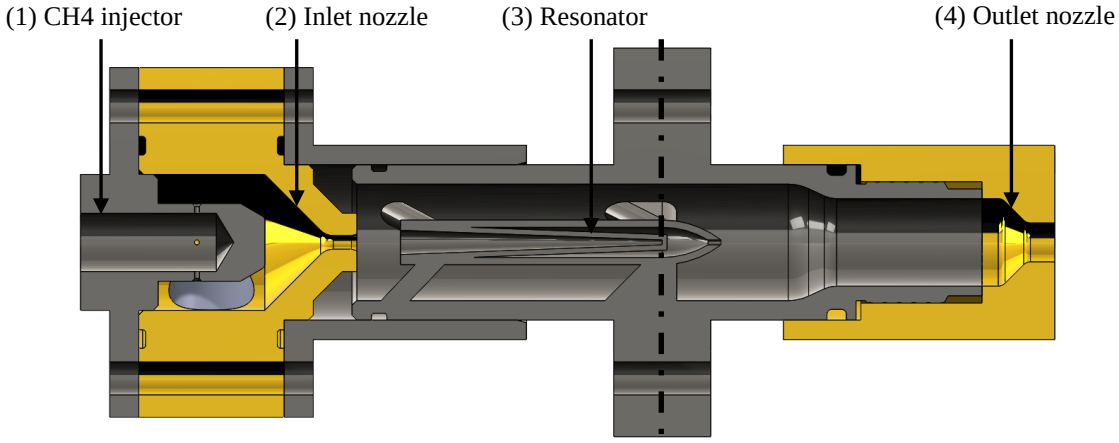


Figure 3: Z2 resonance igniter assembly, half section

In analogy to the revised operational parameters and tests of Z1, the system is designed for choked flow conditions at the inlet nozzle and ignition chamber outlet nozzle both during pre-heating and hot flow. As stated before, this renders the NPR independent of supply pressure, which provides the possibility of igniter operation via a blowdown feed system with supply pressure decreasing over time and also allows the igniter to operate at the same conditions regardless of ambient pressure, from sea level to vacuum. Additionally this means that the extended s/d range viable for resonance of a coax type inlet nozzle is not required, allowing the use of a conventional type inlet nozzle. Such a nozzle is installed in the current Z2 design. The reason for this is a preceding series of ignition run-in tests with the Z2 using a coaxial type nozzle similar to Z1, showing highly unreliable ignition behaviour despite reproducible resonant heating characteristics. This indicates a failure of the system to reliably provide a combustible mix of gases in the hot gas zone at the closed end of the resonator. One probable reason for the poor mixing with a coaxial nozzle in the Z2 compared to the Z1 is the higher mixing time in the Z1, as the jet velocity is comparable yet the distance from nozzle exit to the resonator end is about 3 times longer for Z1. Subsequently, it was decided to inject the methane directly into the inlet nozzle manifold to allow an already partially pre-mixed gas to enter the resonator. In order to enable diameter variation and thus testing of different nozzle pressure ratios, the system features an interchangeable outlet nozzle.
The resonator cavity geometry is a truncated cone with proportions close to the guidelines presented in [10] and similar to the cavity design of the Z1 igniter. The guidelines are applied to the ratio of injection nozzle diameter to resonator inlet diameter for the Z2 initial design with the coaxial injection nozzle. However, a conventional nozzle with the same exit diameter requires substantially more mass flow, thus smaller diameter conventional nozzles are examined. Further the ratio between surface and thus heat losses, and volume of the resonator, decreases with increasing size, so the decision was to keep the oversize resonator for a favourable trade-off between low propellant mass flow and low heat losses. A large resonator is also advantageous considering wall roughness, boundary layer effects and also manufacturability. To further limit convective heat flux from the resonator tube outside wall to the

DOI: 10.13009/EUCASS2019-651



surrounding gas, a hull is set around the resonator. For manufacturing reasons this hull features a bore at the downstream end.
The nominal design parameters of the Z2 igniter are shown in Table 1.

Table 1: Z2 design parameters

| | |
|---|---|
| Ignition chamber interior diameter | 12 mm |
| O2 supply pressure | 18 bar |
| O2 mass flow | 7.2 g/s |
| Oxidizer / fuel ratio | 30 |
| Ideal characteristic velocity (cold) | 406.8 m/s |
| Ideal characteristic velocity (hot) | 1015.5 m/s |
| Combustion temperature | 1682 K |
| Thermal power | 12 kW |

The oxygen supply pressure was chosen as to provide a wide range of NPR combined with a choked outlet. The oxidizer/fuel ratio, or O/F, was set to 30 in order to retain a margin to the lean flammability limit at O/F = 36 and still allow relatively moderate combustion temperatures to prevent hardware damage. The ratio of characteristic velocities $c^*$ equals the ratio of chamber pressures $p_c$ between reacted (hot) and unreacted (cold) gas flow according to **(2)**.

$$c^* = \frac{p_c A_t}{\dot{m}} \quad \textbf{(2)}$$

Here, $\dot{m}$ is the total mass flow and $A_t$ is the cross section of the outlet nozzle. The thermal power of the igniter is determined by the mass flows of both propellants and the total enthalpy difference between unburnt gases and combustion products.
The sensor positions for the Z2 are shown in the section view of Figure 4, with the black chain line in Figure 3 indicating the axial position of the section.

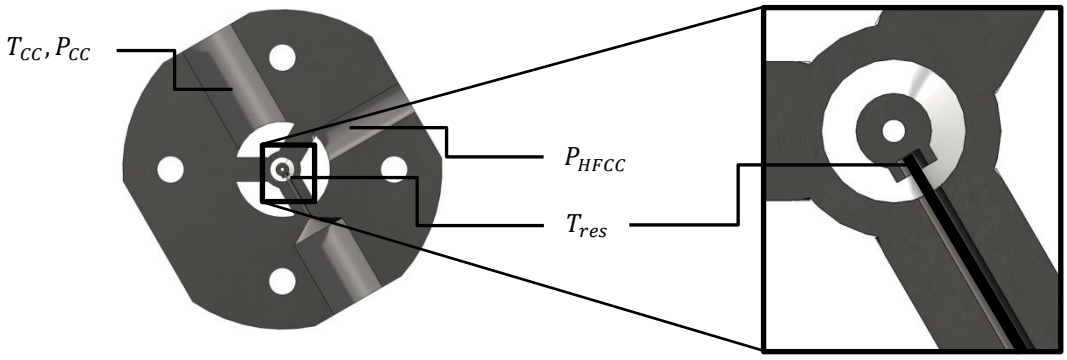


Figure 4: Z2 sensor port section view

The pressure measurement in the chamber, $P_{CC}$, allows determining the NPR of the igniter as well as a verification of the choke condition at the outlet nozzle. Together with the thermocouple $T_{CC}$, ignition detection is possible. The high frequency pressure transducer $P_{HFCC}$, sampled at 50 kHz, provides means to analyse the resonant acoustic modes. A thermocouple $T_{res}$ is installed at the outside wall of the resonator tip for examination of resonant heating performance.
While most parts of the ignition system were manufactured from brass or stainless steel, the ignition chamber holding the resonator is additively manufactured in an SLM process from a Chrome-Cobalt-Molybdenum alloy. This material provides extreme durability and corrosion resistance at high temperatures [19]. The grain size of the additive manufacturing powder used is 10-45 µm.

DOI: 10.13009/EUCASS2019-651



## 5. Test campaign

Finding the optimum configuration for the ignition system in terms of resonant heating is the first target of the presented test campaign. For this, O2 pre-heating tests are conducted and the resonant heating performance is evaluated in relation to variations in NPR, s/d ratio, O2 supply pressure, inlet nozzle expansion ratio and inlet nozzle diameter. Additionally, the correlations between measured acoustic modes and heating performance are examined and discussed and the thermal performance of the new nozzle configurations is compared against the baseline coaxial nozzle of the initial Z2 design. Finally, the results of a preliminary ignition test are outlined.

### 5.1. Test infrastructure and procedures

The test fluid infrastructure shown in Figure 5 provides the working gases for the test article. The propellants are oxygen and methane, and nitrogen is used as an inert gas for purging supply lines and ignition chamber after operation.

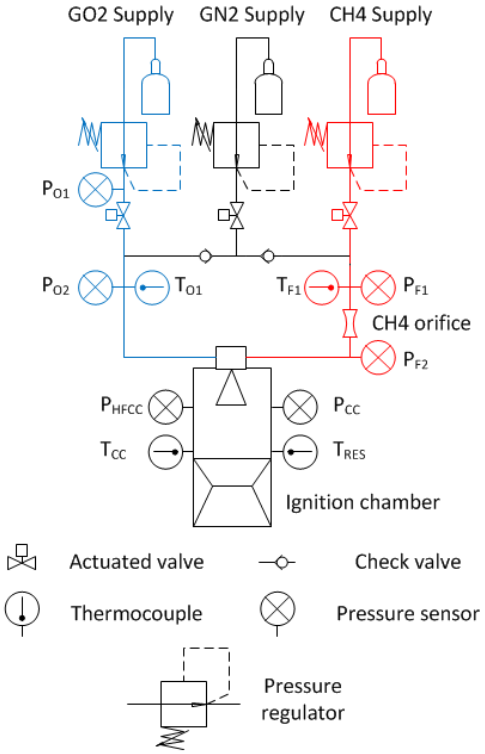


Figure 5: Test rig fluid plan (simplified)

For each feed line there is a pressure regulator installed downstream of the supply followed by an actuated valve. Check valves are installed to prevent the flow of one propellant to the other propellant line through the purge lines. Oxygen mass flow is calculated at the choked inlet nozzle according to **(3)**, [20].

$$C_d = \frac{\dot{m}\sqrt{RT}}{pA\sqrt{\kappa}} \qquad \textbf{(3)}$$

Here $\kappa$ is the isentropic exponent, $R$ is the specific gas constant, $A$ is the cross-sectional area of the choked orifice/nozzle, $C_D$ is the discharge coefficient, $P$ static pressure and $T$ static temperature in the orifice. The latter two are obtained from total pressure and temperature with isentropic correlations. Assuming isentropic expansion through the nozzle, adiabatic conditions and negligible velocity in the feed line, $P_{O2}$ and $T_{O1}$ equal total pressure and respectively total temperature in the orifice. In analogy to this, **(3)** is used to calculate methane mass flow at the CH4 orifice, using pressure $P_{F1}$ and temperature $T_{F1}$. $C_D$ is assumed as 1 for the inlet nozzle, as other orifices of comparable diameter and inlet contour were experimentally examined to yield a discharge coefficient around 99%, while for the far smaller CH4 orifice, $C_D$ was found to be 0.94 in calibration tests. Note that with both methane and oxygen flowing at the same time, a change in oxygen mass flow is expected since a mixture is flowing through the inlet nozzle. However, this is considered as negligible regarding the high O/F ratio of 30, yielding an error of about 3%. The sensor PF2 is used to measure the CH4 injector pressure and to verify if critical flow conditions are present

DOI: 10.13009/EUCASS2019-651



at the CH4 orifice. Actuator control and data acquisition are performed on a real time system connected to a PC for control and data storage. On this test infrastructure, both pre-heating and ignition tests are performed. Figure 6 shows sensor data from a typical pre-heat test. The oxygen valve opens for 5 seconds as indicated by the pressure data from the oxygen feed line and the igniter chamber. In this timeframe resonator temperature rises until the valve is closed. Note that resonator temperatures measured by $T_{res}$ are only for qualitative comparison between test cases. The resonator wall thickness is 0.5 mm and the thermocouple tip is held against the wall by a compression fitting. The total thermal resistance between the thermocouple and the resonance gas is not known and they do not represent actual gas temperatures in the resonator.

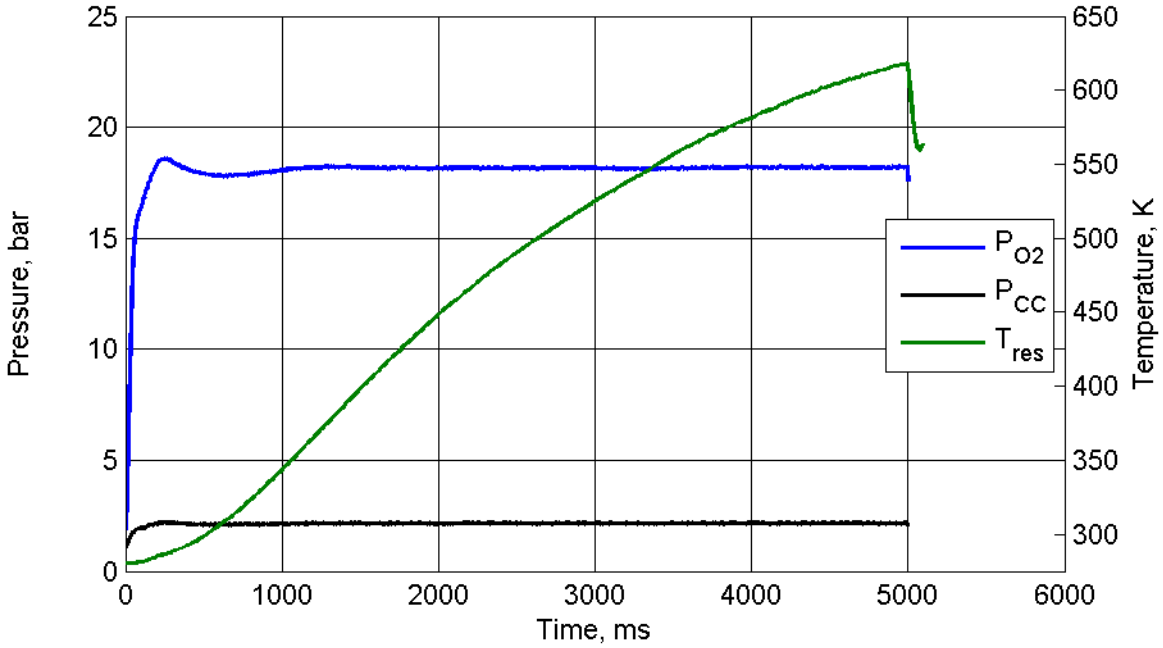


Figure 6: O2 pre-heat sequence data

## 5.2. Heating performance evaluation

The primary heating performance tests are conducted at the nominal mass flow and 18 bar supply pressure which is obtained with a nozzle throat of 1.4 mm. Two inlet nozzles are investigated: One with convergent contour, in the following named Type A, and one with de Laval contour and an expansion ratio $\varepsilon$ = 1.5, designated Type B. The expansion ratio is defined as nozzle exit area divided by nozzle throat area. For Type A the free jet Mach number is 1 and for Type B the Mach number is 1.85.

Figure 7: Inlet nozzle contours: Type A (left), Type B (right)

For the variation of NPR, outlet nozzle diameters from 3.25 to 5 mm diameter were used. Not all possible combinations are tested since below NPR = 5 the inlet nozzle loses critical flow condition with chamber pressure rising during hot gas operation of the igniter and above NPR = 9 the outlet nozzle loses critical flow condition at the supply pressure of 18 bar. The pre-heat tests consist of an oxygen supply valve opening for 5 seconds, and the criterion to compare heating performance between different test points is the maximum temperature reached at $T_{res}$ within this time frame. To ensure consistent test results, a set of guidelines was applied to the entire campaign. Before each test, $T_{res}$ must be below 290 K and $P_{O2}$has to be within ± 0.3 bar of the nominal value, which is verified in a flow check before a test series. Also, for all tests, O2 inlet temperatures are within a 15 K range. In this temperature interval, a clear correlation between initial resonator temperature, gas inlet temperature and maximum heat up temperature was not found. For this reason it was decided to show absolute temperatures instead of

DOI: 10.13009/EUCASS2019-651



differences between maximum $T_{res}$ and e.g. resonator temperature at the start of the test. For each tested inlet/outlet nozzle combination, the nozzle-resonator distance resolution between test points is 0.5 mm for maximum values of $T_{res}$ < 500 K and 0.25 mm for $T_{res}$ > 500 K to have more detailed information in the areas of high resonant heating. Also, for each inlet/outlet nozzle combination, the nozzle-resonator distance or s/d yielding the highest maximum $T_{res}$ is tested in a repetition. After one inlet nozzle is tested with all reasonable outlet nozzles, the tests are repeated again twice for the s/d with the highest maximum $T_{res}$. Contrary to the plan in Figure 5, for the pre-heat tests the methane line was closed upstream of the injection nozzle to prevent O2 backflow into the methane line, affecting the pressure rise in the nozzle manifold at start-up.
An evaluation of attained maximum resonator temperatures for the Type A and Type B nozzle over s/d for various NPR is given in Figure 8. The shown NPR values are averaged for the respective test series since there are deviations between individual tests. However, these are minimal with a highest relative deviation of less than 2.5%.

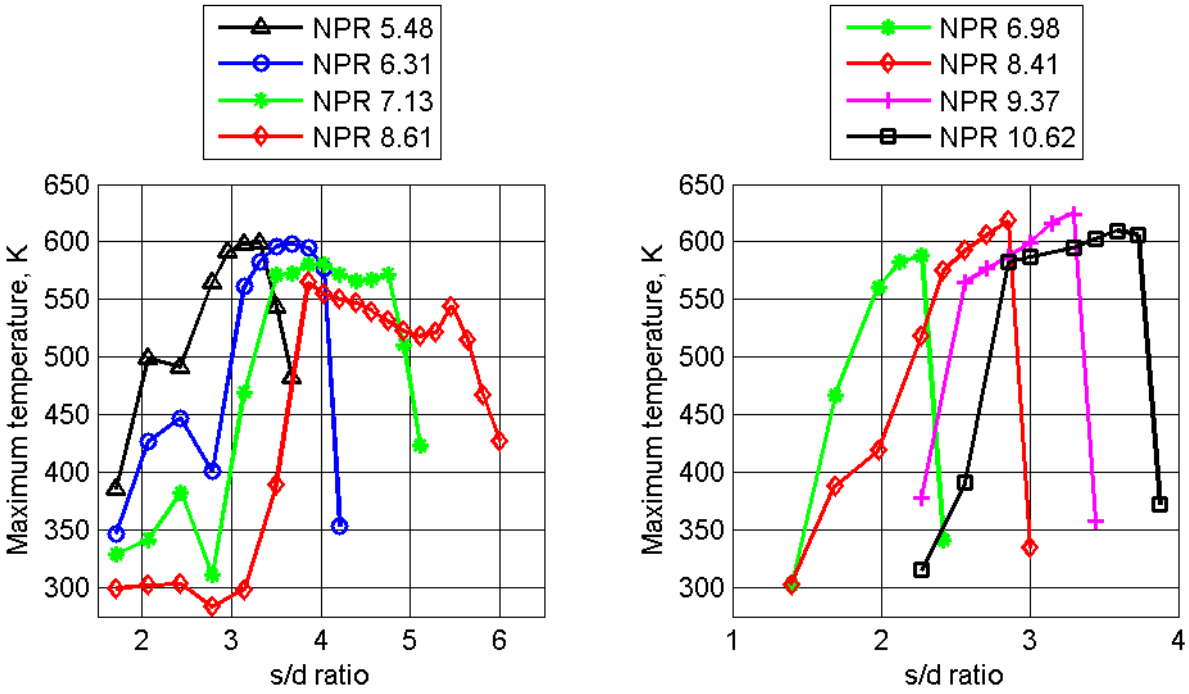


Figure 8: Heating performance for Type A (left) and Type B (right) inlet nozzle

The Type B nozzle shows improved heating performance over Type A and the NPR optimum for Type B is higher at around 9 compared to Type A with an optimum around 6. For each NPR shown, a steep increase in maximum temperature over increasing s/d indicates the onset of a resonant mode. Further increase of s/d leads through a zone of generally high attained maximum temperatures followed by an abrupt decrease in temperature. It is observed for both nozzles that with increasing NPR, these s/d zones for high heating performance shift to higher s/d values and their ranges expand, forming a plateau of approximately constant temperature rather than a distinct maximum point. As stated in section 2, to obtain a resonant operation in the jet regurgitant mode (JRM), the nozzle-resonator distance needs to be equal or larger than the nozzle-shock distance of the free jet [12]. Thus, it shall be verified if the observed steep temperature increase over increasing s/d is caused by JRM. To analyse this condition for the present tests, maximum temperatures are shown in relation to s/d ratio and NPR for both nozzle types in Figure 9 together with the position of the free jet shock relative to NPR. The length of the free jet shock structure divided by nozzle exit diameter, $X_s/d$, is calculated according to the semi-empirical correlations **(4)** and **(5)** elaborated in [21] and further outlined in [22]:

$$X_s/d = 1.55\left(M_d^2\frac{p_d}{p_u} - 1\right)^{0.5} - 0.55(M_d^2-1)^{0.5}, for\ \frac{p_d}{p_u} \leq 2 \qquad \textbf{(4)}$$

$$X_s/d = 1.52\left(\frac{p_d}{p_u}\right)^{0.437} + 1.55[(2M_d^2-1)^{0.5} - 1] - \\ - 0.55(M_d^2-1)^{0.5} + 0.5\left\{\frac{1}{1.55}\left[\left(\frac{p_d}{p_u} - 2\right)(M_d^2-1)^{0.5}\right]^{0.5} - 1\right\}, for\ \frac{p_d}{p_u} > 2 \qquad \textbf{(5)}$$

DOI: 10.13009/EUCASS2019-651



Here $p_u$ is the ambient pressure surrounding the jet. The static pressure of the jet $p_d$ is obtained by the jet Mach number $M_d$ and jet total pressure. According to the fields of application presented, equation **(5)** is used for the Type A nozzle and equation **(4)** for Type B. In the upper frame of Figure 9, $X_{s,2}$ is the distance of the second shock structure, assumed to be double the distance of the first one.

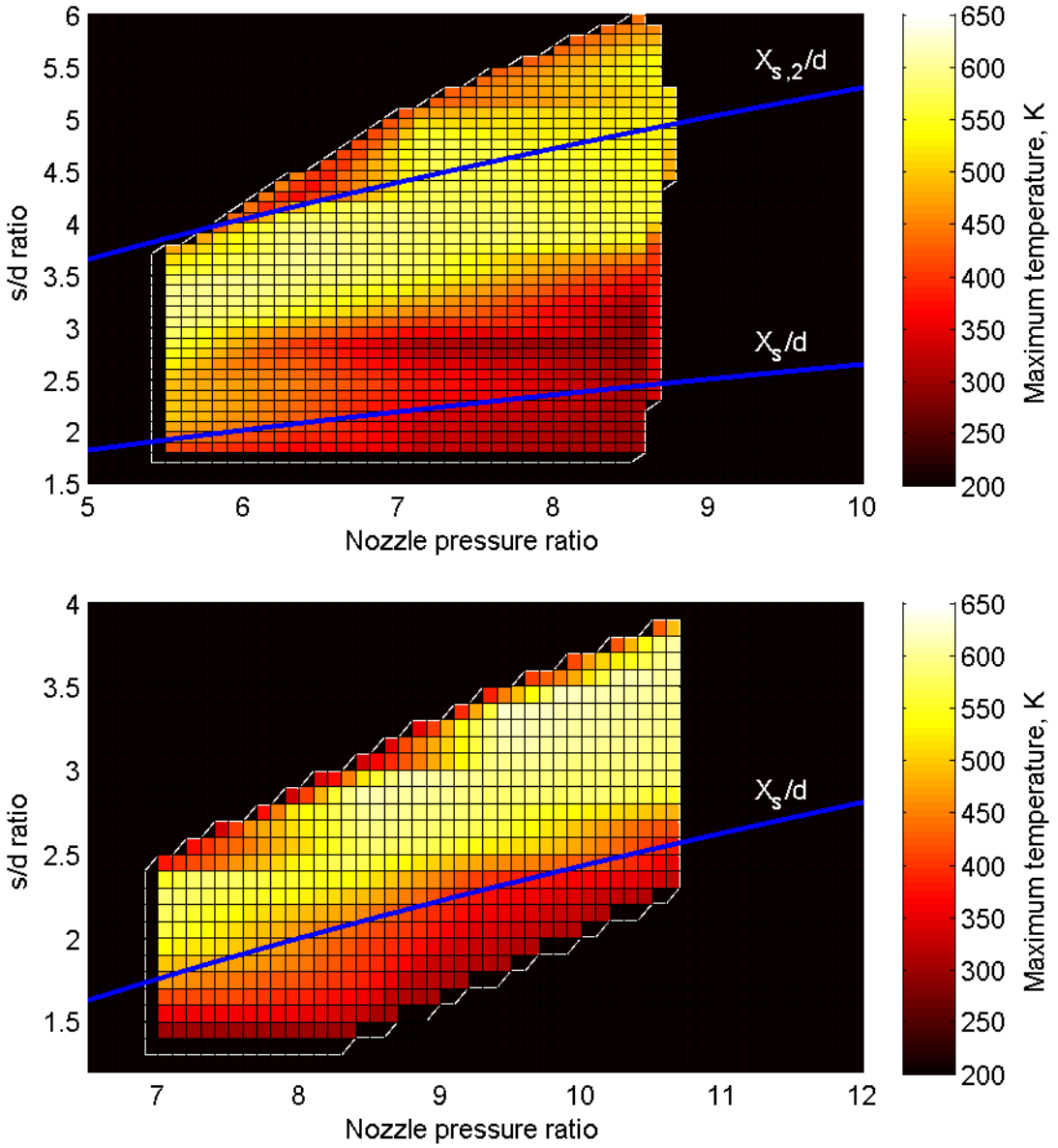


Figure 9: Maximum pre-heat temperatures over NPR and s/d ratio. Above: Type A nozzle, Below: Type B nozzle

It is shown that for the Type B nozzle, $X_s/d$ is located below the points where temperatures increase steeply with increasing s/d, indicating that JRM is the heating mechanism according to [12]. In contrast to this, for the Type A nozzle the expected $X_s/d$ for JRM is located roughly between the calculated first and second positions. However, these correlations hold an uncertainty, which can be outlined by comparing the calculated shock positions with experimental data shown in Figure 10, [12], which yields 10-20% lower values for $X_s/d$. Since the transition from JSM to JRM is also observed at shock cells beyond the first one [12], it is assumed that Type A transitions from JSM to JRM from $X_{s,2}/d$ to higher s/d. Figure 10 outlines the transition from jet screech mode (JSM) to JRM at the position of the free jet shock structures up to an NPR of 6. With higher NPR, the transition border no longer follows $X_s/d$ but moves up to higher distances. In this NPR region the formation of temperature plateaus, at NPR of 7.13 and 8.61, is observed in Figure 8, although no connection can be proven between the two phenomena. For the Type B nozzle, no direct conclusions can be drawn from Figure 10 since the data presented there is valid for a jet Mach number of 1 from a convergent nozzle. Still, it is observed that for Type B the formation of the plateaus as seen for the Type A nozzle starts at higher NPR, see NPR = 10.62 in Figure 9, and that the transition point from JSM to JRM

DOI: 10.13009/EUCASS2019-651



is still at $X_s/d$, even at NPR higher than 6. It is therefore assumed that these two effects are connected and are caused by the higher inlet Mach number, yet no further investigations have been conducted on the subject.

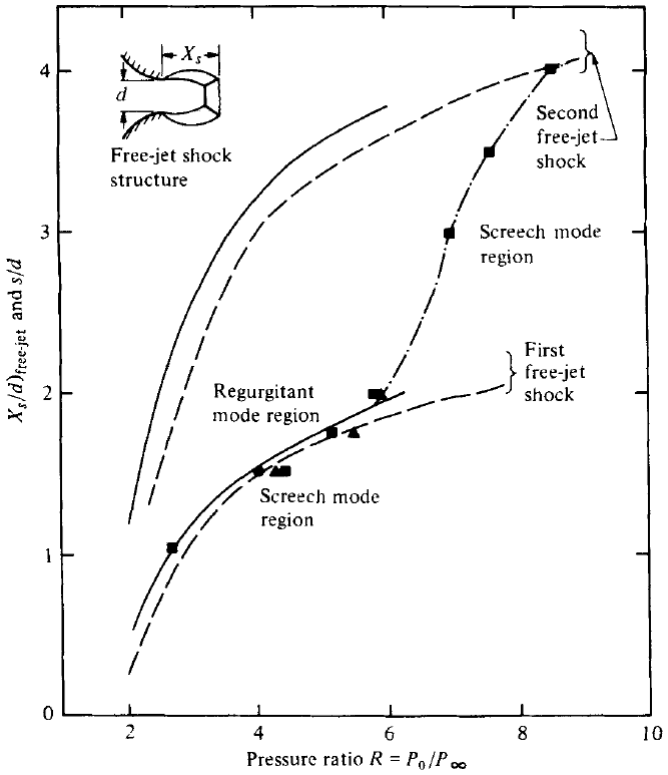


Figure 10: Regions of resonant tube operation [12]

In order to identify the resonant modes of operation an acoustic analysis is carried out for nozzle Type A and B. As stated in section 2, the JRM operates at the Eigen frequency of the resonator cavity, which is calculated according to **(6)**, [23]. Here, x is the truncated length of a virtual full cone [23], defined in **(7)**, and $v(T)$ is the speed of sound.

$$\frac{2\pi f_{0,cone}}{v} L = \pi - arctan\left(\frac{2\pi f_{0,cone}}{v(T)} x\right) \quad \textbf{(6)}$$

In **(7)**, $D_2$ and $D_1$ are respectively the beginning and end diameter of the conical resonator cavity and $L$ is the length of the cavity.

$$x = L\frac{D_1}{D_2 - D_1} \quad \textbf{(7)}$$

As gas properties within the cavity are not precisely available, inlet nozzle properties are assumed for the calculation, yielding an estimate value for the Eigen frequency of the conical resonator cavity. Equation **(6)** was numerically solved, the input and output data is given in Table 2.

Table 2: Resonator Eigen frequency calculation parameters

| | | | | | |
|---|---|---|---|---|---|
| $D_1$ = 0.5 mm | $D_2$ = 2.4 mm | $L$ = 26.2 mm | $P$ = 18 bar | $T$ = 280 K | $f_{0,cone}$ = 4935 Hz |

A Fast Fourier Transform (FFT) is performed with the high frequency pressure data from the sensor $P_{HFCC}$ for the tests series of the Type A and B nozzles. The signal is processed by a Blackman window and the FFT window length used is $2^{12}$ = 4096. Figure 11 shows the signal amplitude over frequency and measured s/d for the nozzle Type B at an NPR of 8.41, together with the attained maximum temperatures at the corresponding s/d values. The amplitude is visualised as a colour map for qualitative comparison with that data points interpolated over a grid. In the s/d range from 1.7 to 2, high frequency oscillations from 12 to 20 kHz dominate. This, combined with a moderate heating effect is attributed to the JSM, which shows a varying frequency in relation to s/d [12]. The s/d regime from 2.3 to 2.9 shows high amplitude oscillations at a frequency of about 4.6 kHz, which is assumed to be the fundamental

DOI: 10.13009/EUCASS2019-651



frequency of the resonator, as it deviates by only 7% from the calculated value. This strongly indicates JRM operational mode, which is further consolidated by the high temperatures measured for these s/d.

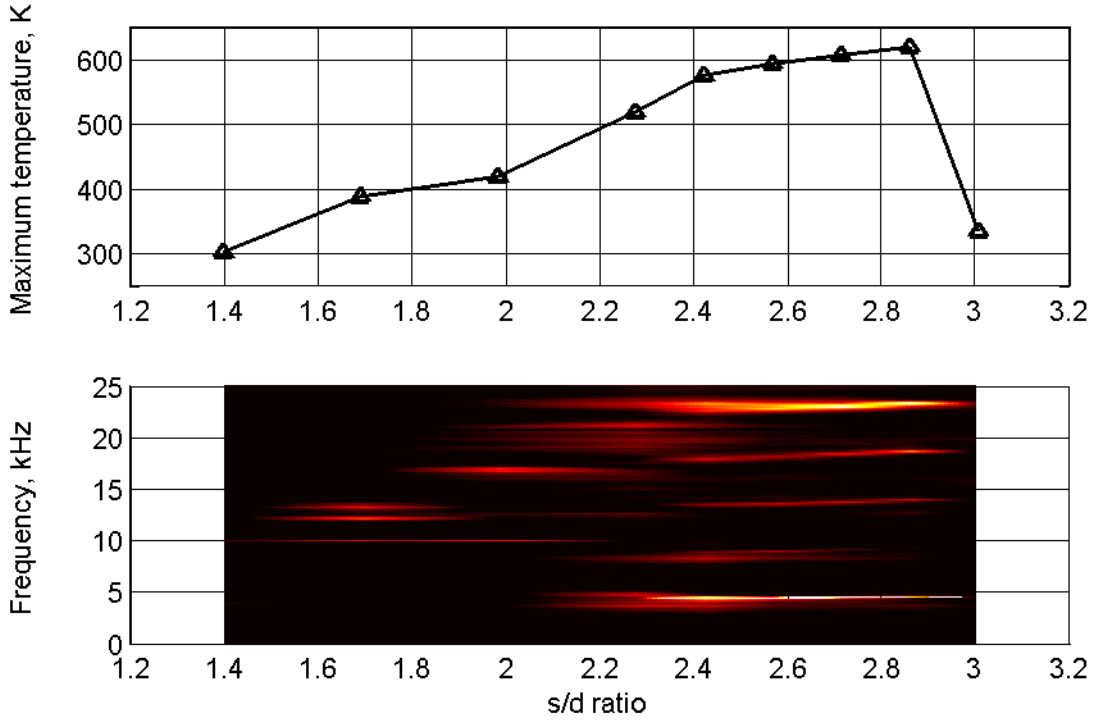


Figure 11: Frequency spectrum and maximum temperature over s/d ratio at NPR 8.41, Nozzle B

In analogy to this, Figure 12 displays the frequency analysis of the Type A nozzle at NPR = 6.31. Here, JSM operation is indicated for s/d between 1.7 and 2.8 while the JRM zone spans from roughly 3.2 to 4.1.

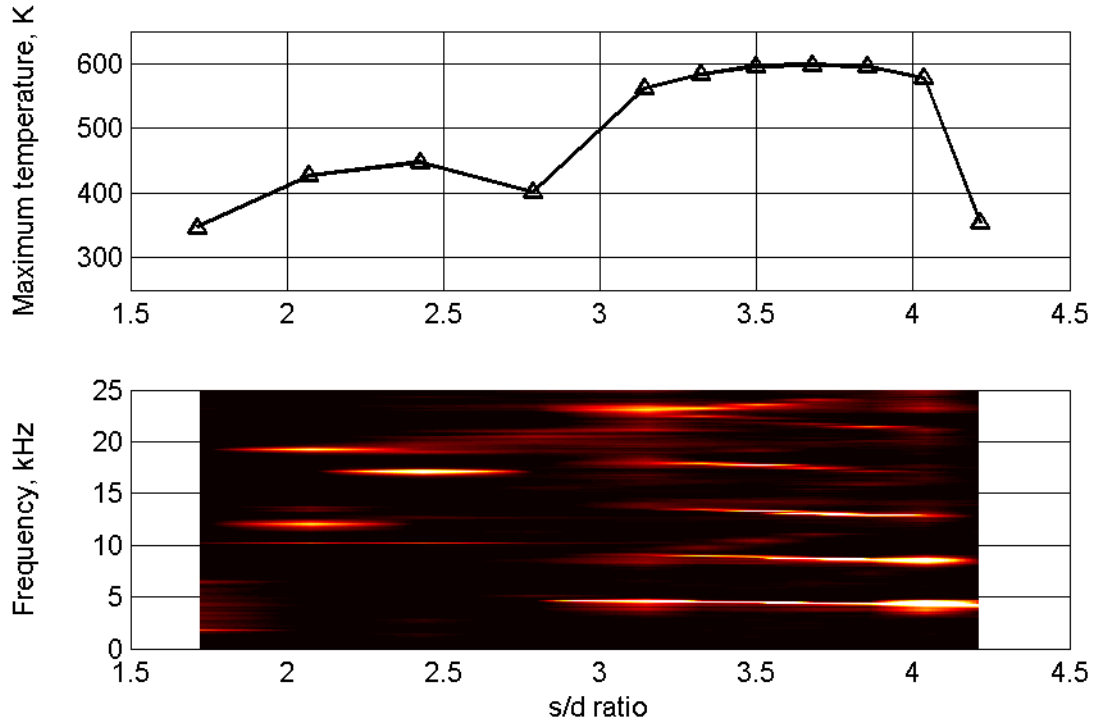


Figure 12: Frequency spectrum and maximum temperature over s/d ratio at NPR 6.31, Nozzle A

Figure 13 shows an onset of JSM at comparatively high s/d of about 3.5 to 4. From s/d = 3.5 to 5.5, the high amplitude peak of the fundamental frequency and the first harmonic dominate as well as high amplitude peaks from

DOI: 10.13009/EUCASS2019-651



20-25 kHz. The narrow peaks observed at approximately 10 kHz from Figure 11 to Figure 13 cannot be assigned directly to an operating mode. Although their appearance is primarily in the JSM regime, their constant frequency over s/d is untypical for that mode. Possible causes include disturbances on the measuring track, aliasing effects or excitation of other geometrical structures in the ignition chamber, yet this effect is not further investigated.

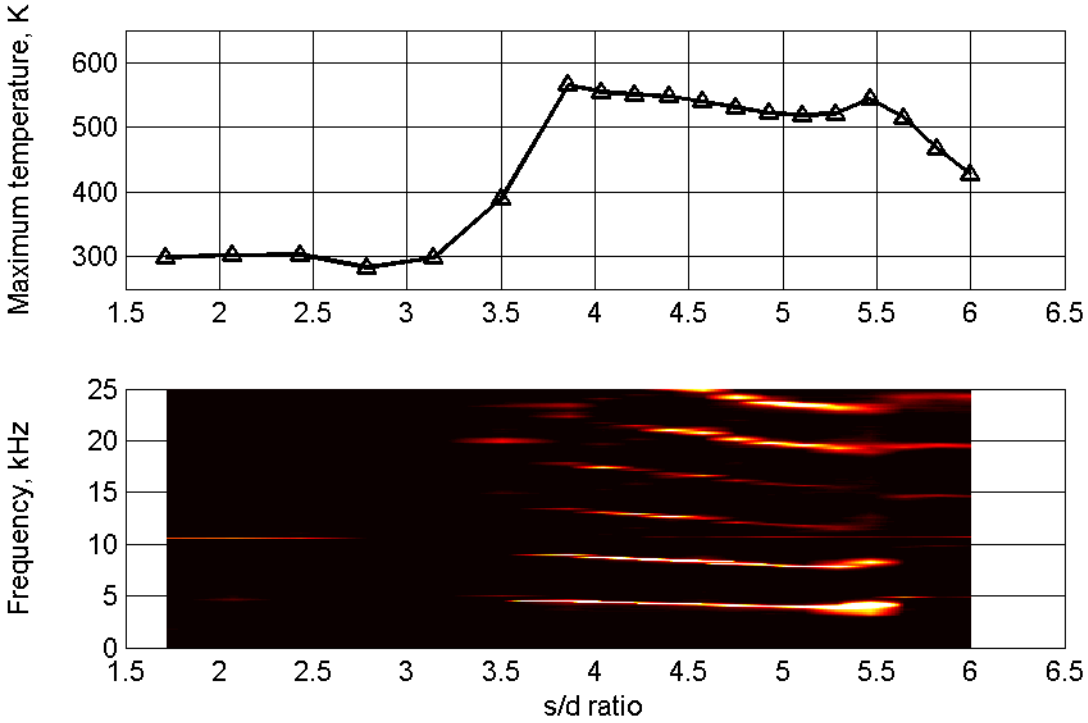


Figure 13: Frequency spectrum and maximum temperature over s/d ratio at NPR 8.61, Nozzle A

The results strongly support the assumption that the type A nozzle transitions from JSM to JRM at the position of the second free jet shock, for NPR = 6.31. According to the presented data the operating mode of Type A at NPR = 8.61 is not clearly identified and a persisting state of transition between JRM and JSM over the plateau is assumed. For the Type B, a transition from JSM to JRM at the position of the first free jet shock structure is indicated.
In the extended test series, variants of the Type A nozzle with 1.5 mm and 2 mm throat diameter and a variant of the Type B with 1.5 mm throat diameter and $\varepsilon = 1.5$, as well as the coaxial nozzle are tested in procedures according to the primary test campaign. Figure 14 shows a summary of the maximum temperatures at the respective optimum s/d ratio for the nozzle pressure ratios tested on each inlet nozzle.

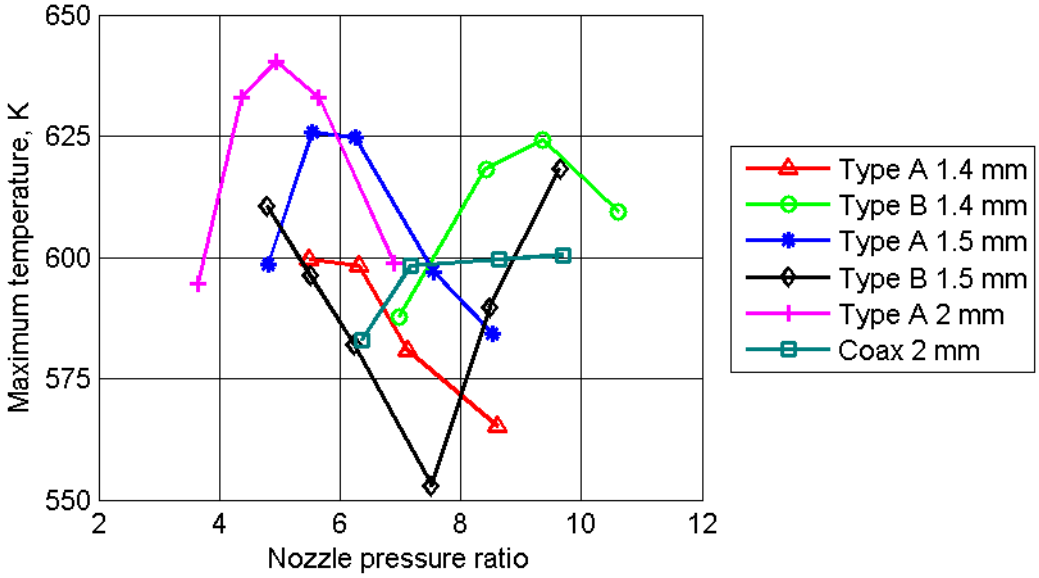


Figure 14: Extended test series inlet nozzle heating performance

DOI: 10.13009/EUCASS2019-651



The Type A nozzles with 2 and 1.5 mm diameter show a temperature increase compared to the 1.4 mm nozzles, however double or respectively 15% more mass flow is required for operation which is an unfavourable trade-off, so these two options are dismissed for the final configuration. The same argumentation applies to the 1.5 mm Type B nozzle, which additionally lacks the advantage of higher attained temperatures compared to the 1.4 mm nozzles. Finally, the 1.4 mm Type B nozzle is selected over the Type A nozzle for higher heating performance. Also, comparing this to the initial coaxial nozzle, significant improvements in heating performance are gained. Together with the increased manufacturing difficulty of the coax nozzle, including higher requirements for geometrical tolerances, the latter is rendered as not viable. For the final configuration the outlet nozzle with 4 mm diameter is selected, yielding the NPR of 8.41. Although the heating performance for this NPR is marginally lower than for 9.37, it provides more margin for sustaining the outlet critical pressure ratio at lower supply pressures since the igniter chamber pressure is slightly higher.

Over the course of the extended test campaign a series of anomalies has been encountered from which the most relevant shall be outlined here. During a series of run-in tests, optimum temperatures for the Type A nozzle at NPR = 6.31 were on par with optimum temperatures obtained with Type B. For the Type A at this particular NPR, the maximum attained temperature at the optimum s/d is about 30 K lower in the here presented final test series, while other NPR remained unaffected. Despite thorough investigation, the cause for this behaviour was not identified. The other test series were highly reproducible with the repetition tests in the optimum s/d and NPR for each inlet nozzle showing deviations of no more than 5 K.

For all Type A nozzles JRM is obtained with s/d near the position of the second shock structure. Only for the Type A nozzle with 2 mm diameter JRM is recorded at the first and second shock structure. In contrast to the smaller Type A nozzles, with the 2 mm nozzle the ratio of resonator inlet diameter to nozzle diameter is according to the guidelines presented in [10], which might explain the ability of this particular configuration to trigger JRM at the first shock structure position. However, overall no improved heating performance is observed at the first shock, so the operation at the second shock is not considered as a disadvantage.

For the 1.5 mm Type B nozzle a significant drop in heating performance is visible at an NPR of 7.51 in Figure 14. It is stated in [16] that a resonator configuration without a coaxial insert in the nozzle relies on the presence of shock cells for operation. It is suspected that for the operation at NPR = 7.51 the jet is near ideal expansion, thus no shock structure is formed. At the nominal expansion ratio of 1.5 for the Type B nozzle, the static pressure of the jet drops by a ratio of 6.24, yet an increase of the outlet diameter by only 5% already yields a jet pressure ratio of 7.5, thus providing ideal expansion, which is possible considering the size of the device and the corresponding manufacturing limits. Therefore it is assumed that said drop in heating performance is caused by near ideal expansion of the jet. This phenomenon might also explain the low performance of the Type B 1.4 mm nozzle at an NPR of 6.98. At NPR lower than 7.51, the 1.5 mm Type B nozzle shows increasing heating performance, however these operating points were not further investigated since these low NPR provide insufficient margin to hold the choke condition of the inlet nozzle during ignition, see also section 5.2.

A regular pattern that was found is that the formation of temperature plateaus at high NPR for the 1.4 mm Type A and B nozzles is also observed with the 1.5 mm nozzles and the 2 mm Type A nozzle. For Type A nozzles the phenomenon manifested at NPR beyond 6 and for Type B beyond 9.

With the final configuration, Type B 1.4 mm nozzle and 4 mm outlet nozzle, heat-up tests were performed for varying inlet pressures in a narrow range of nozzle-resonator-distances. The maximum achieved temperatures and the nozzle pressure ratio over inlet pressure are shown in Figure 15.

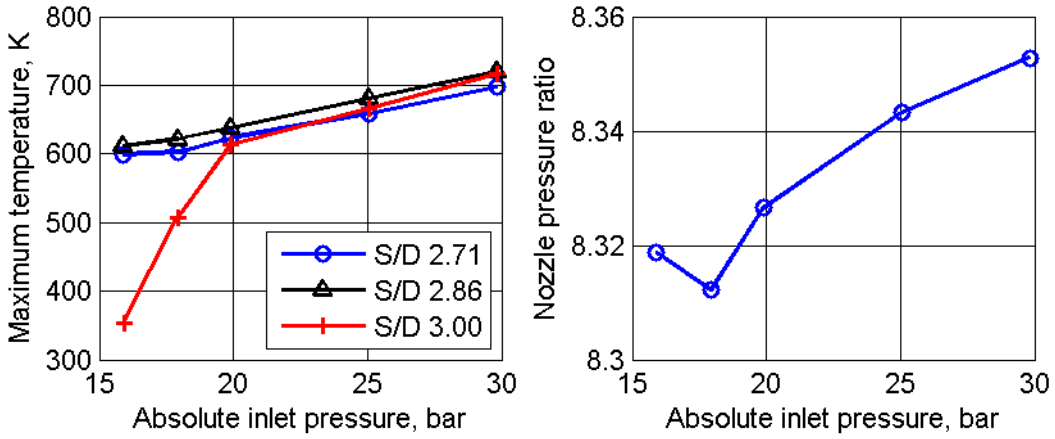


Figure 15: Resonant heating performance and NPR over inlet pressure for final igniter configuration

DOI: 10.13009/EUCASS2019-651



It is outlined that within practically useful pressure ranges, the NPR remains nearly constant, showing a minimal increase over supply pressure. The tests at s/d = 3.00 are near the transition border beyond which resonant operation ceases. The increase in NPR over inlet pressure shifts this distance towards optimum, however this effect is marginal and cannot fully explain the shift towards the resonant regime. Also in other test cases it was observed that the range of distances where resonance occurs generally enlarges with higher inlet pressure, e.g. a distance which might be near the transition border for low inlet pressure will move into the resonant regime, given higher inlet pressures. This effect was observed despite fully choked flow in inlet and outlet nozzle, with near constant NPR. Also it is worth mentioning here that during the tests, the resonator distances were set anew between each pressure level, leading to possible distance uncertainties up to ± 0.1 mm. Close to the transition border these uncertainties lead to high temperature deviations between nominally identical test points. While each test was repeated once and the deviations in temperature were in the range of up to 30 K for s/d = 3.00, they are less than ± 3 K for the other two distance settings.
To conclude, a substantial dependency between heating performance and inlet pressure is demonstrated. Further it was shown experimentally that with this configuration the optimum s/d ratio is constant over the relevant range of inlet pressures, which is in accordance with the design. Thus, one of the major restrictions for operating the device via a blowdown type feed system is eliminated.

### 5.3. Ignition tests

A series of ignition tests is performed with the final igniter configuration at s/d = 2.86. The sensor data for a test with an ignition event produced at 25 bar O2 inlet pressure and an O/F ratio of 28 is given in Figure 16. The test sequence is initiated by a pre-heat with oxygen, as shown in the pressure data of $P_{O2}$. Parallel to this, the methane valve is opened shortly, indicated by $P_{F1}$, to fill the methane line and prevent oxygen backflow. This enables a higher fraction of methane exiting the CH4 injector directly when the methane valve opens for a second time.

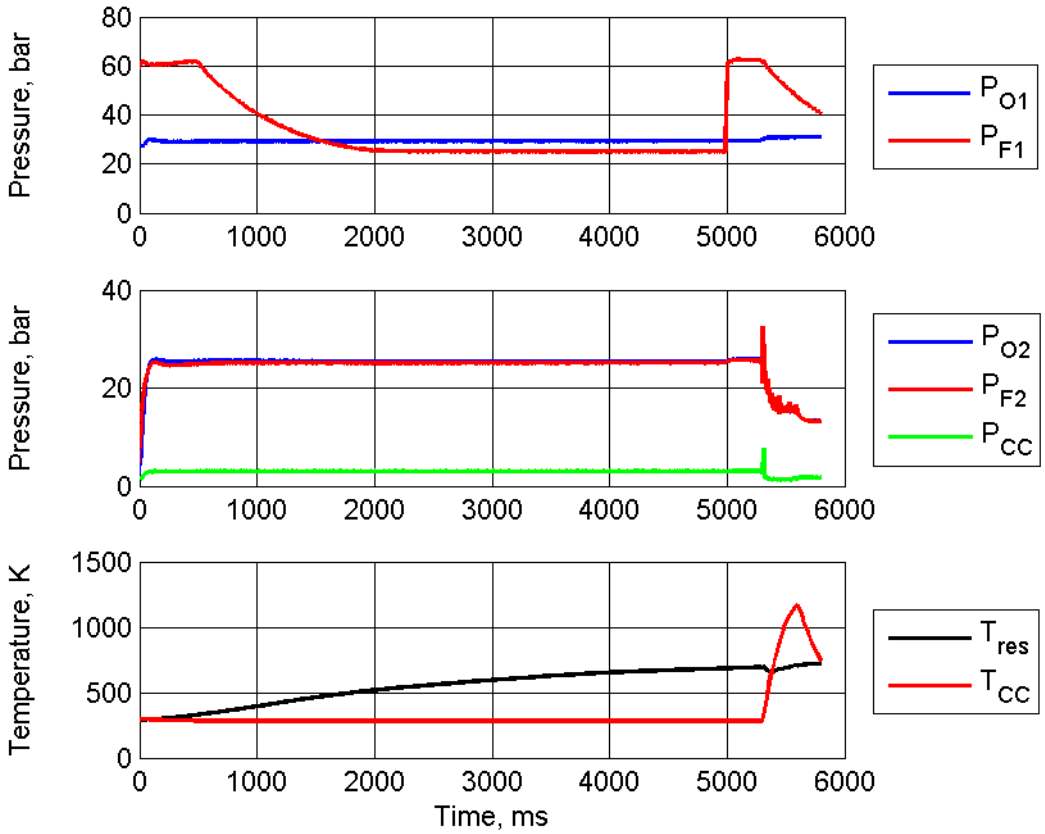


Figure 16: Ignition test sensor data

The second methane valve opening is nominally intended to trigger the ignition, instead the data shows an ignition subsequent to the closing of both methane and oxygen valves, at the time when the nitrogen purge of the chamber is initiated. The reason for the missing ignition at methane valve opening is strongly suspected to be a local excess of

DOI: 10.13009/EUCASS2019-651



oxygen in the hot region of the resonator cavity tip. In this zone, mass exchange is restricted and a gas mixture within flammability limits does not exist at the designated time despite a global O/F ratio of 28. After shutdown, the pressure in the methane line drops slower than in the oxygen line, shifting the O/F to a more fuel-rich mixture in the transient and thus providing a combustible mixture to the resonator tip. Here, despite dropping gas temperature due to shutdown of the resonance operation, ignition is achieved. The high pressure peaks and subsequent pressure fluctuations observed for $P_{CC}$, $P_{O2}$, and $P_{F2}$ indicate a hard ignition with a propagation of the flame front upstream through the inlet nozzle, followed by combustion in the manifold. The hard ignition is caused by the ignition chamber being filled with a combustible mixture due to the flow of both methane and oxygen from the inlet nozzle. This mixture spontaneously reacts after ignition in the cavity and causes the aforementioned pressure peak in the chamber which in turn stagnates the flow from the inlet nozzle. This allows the reaction zone to enter the manifold, igniting the mixture therein.
This ignition mechanism is clearly inefficient as the resonant heating effect is not fully exploited. Also the ignition is not reliable since there are tests conducted under the same conditions without an ignition event. In tests with oxygen supply pressures below 25 bar, no ignition could be observed. The presented igniter operating conditions are not suitable for the ignition of a rocket engine, however, it is clearly demonstrated that the resonant heating performance in this setup is sufficient to produce an ignition.

## 6. Conclusion and future prospects

Based on the acquired data presented in this document, a new system configuration is elaborated for the Z2 igniter with superior heating performance compared to the initial design baseline. It is demonstrated that this system is able to operate at a constant nozzle pressure ratio and thus optimum nozzle-resonator distance, independent of supply pressure variations, which allows the use of a blowdown type gas supply. Additionally the system provides identical operating conditions at varying ambient pressures from vacuum to sea level pressure. Further, the capability of the system to produce ignition of an oxygen/methane mixture is demonstrated.
The observed resonant heating effects are investigated and the impact of particular influence parameters on resonant heating performance is outlined. The increase of inlet nozzle expansion ratio and thus jet Mach number is shown to extend the range of NPR for which a regular transition from JSM to JRM is observed along the position of a free jet shock structure. Heating performance is observed to drop when the jet flow is near ideal expansion conditions. For each tested inlet nozzle, an optimum NPR is determined which is increasing with increasing jet Mach number and decreasing with increasing nozzle diameter. The increase of inlet nozzle diameter and thus nozzle mass flow at a given supply pressure is shown to have a minor positive impact on heating performance. At a nozzle diameter to resonator inlet diameter ratio of 1.25, in accordance with guidelines found in literature, JRM is produced at the first free jet shock structure position with a convergent nozzle, yet no advantage in heating performance is observed compared to the operation at the second shock structure. Further it is shown that the increase of supply pressure has a strong positive impact on resonant heating performance.
Subsequent to these investigations, sequence and load point optimisations will be performed in future igniter tests. As in the presented ignition scenarios the full potential of the resonant heating effect is not utilised yet, significant improvements are possible in terms of reliability, pre-heat time and required supply pressure. Additionally, an ignition chamber and resonator with identical geometry, additively manufactured from partially stabilised zirconium dioxide, shall be examined. Since this material offers a thermal conductivity one magnitude lower compared to the current chrome-cobalt-molybdenum alloy, further ignition performance improvements are expected. Simulations performed by Bauer [24] suggest considerable mass exchange through the resonator hull bore, which in turn increases convective heat flux from the resonator outside wall. Thus, a redesign of the hull geometry might again improve resonant heating.
Following these steps, operational envelopes for the igniter shall be elaborated for constant pressure and blowdown supply conditions. Subsequently, rocket engine start-up tests with this ignition system will be conducted.

## Acknowledgments

The author thanks Munich Aerospace for rendering this project possible and for the support. Additionally, the help at the test facility from the students in the practical course for space propulsion at TU Munich is thankfully acknowledged. Many thanks are also due to Gerhard Giel for first-class quality TIG welds on the igniter hardware.

DOI: 10.13009/EUCASS2019-651



## References


[1] ECHA, “Inclusion of Substances of Very High Concern in the Candidate List,” Helsinki, 2011.

[2] ECHA, „Proposal for identification of a substance as a category 1A or 1B CMR, PBT, vPvB or a substance of an equivalent level of concern,“ 2011.

[3] The European Parliament and the Council of the European Union, „REGULATION (EC) No 1907/2006 OF THE EUROPEAN PARLIAMENT,“ 2006.

[4] C. Muratov, V. Osipov and V. Smelyanskiy, “Issues of Long-Term Cryogenic Propellant Storage in Microgravity,” National Aeronautics and Space Administration, NASA Ames Research Center Moffett Field, CA, 2011.

[5] D. Plachta, W. Johnson and J. Feller, “Zero boil-off system testing,” Elsevier Cryogenics, 2015.

[6] C. Bauer, J. Pauw and O. J. Haidn, “Numerical and Experimental Investigations on Resonance Ignition,” 2014.

[7] P. Lungu, C. Bauer and O. J. Haidn, “Operational behaviour investigation of Hartmann-Sprenger Tube based resonance ignition systems for oxygen/methane in-orbit propulsion applications,” in *Space Propulsion 2018*, Sevilla, 2018.

[8] J. Hartmann, „On a new method for the generation of sound-waves,“ *Physics Review, Vol. 20, No. 6,* 1922.

[9] H. Sprenger, „Über thermische Effekte in Resonanzrohren,“ *Mitteilungen aus dem Institut für Aerodynamik and der ETH Zürich,* 1954.

[10] B. R. Phillips and A. J. Pavli, “Resonance tube ignition of hydrogen-oxygen mixtures,” NASA Lewis Research Center, Cleveland, Ohio, 1971.

[11] E. Rakowsky, A. Corrado and V. Marchese, “Fluidic explosive initiator,” *Fluidics quarterly,* vol. 6, no. 1, 1974.

[12] V. Sarohia and L. Back, “Experimental Investigation of Flow and Heating in a Resonance Tube,” *J. Fluid Mech.,* no. 94, 1979.

[13] L. Stabinsky, “Analytical and Experimental Study of Resonance Ignition Tubes,” Rocketdyne Division, 1973.

[14] Y. Song, N. Yu, G. Zhang, B. Ma, W. Zhou and X. Huang, “Investigation of Novel Hydrogen/ Oxygen Thruster for Orbital Maneuver in Space Station,” *Chinese Journal of Aeronautics,* 2005.

[15] K. Kessaev, M. Niwa and A. Santana Jr., “Development of a Resonance Igniter for GO2/Kerosene Ignition,” *Journal of Propulsion and Power,* September-October 2001.

[16] E. Brocher and J. Ardissone, “Heating characteristics of a new type of Hartmann-Sprenger tube,” *Int. J. Heat & Fluid Flow,* vol. 4, no. 2, 1983.

[17] C. Bauer, M. Hauser and O. Haidn, “Investigation of Stabilization Effects in Hartmann-Sprenger-Tubes,” in *30th International Symposium on Space Technology and Science (ISTS)*, Kobe, 2015.

[18] C. Bauer and O. J. Haidn, “Design and Test of a Resonance Ignition System for Green In-Orbit Propulsion Systems,” 2016.

[19] citim GmbH, *Datenblatt Selektives Laserschmelzen (SLM), Kobalt-Chrom-Molybdänlegierung CoCrMo,* Barleben, 2016.

[20] M. P. Celano, S. Silvestri, G. Schlieben, C. Kirchberger and O. Haidn, “Characterization of a GOX-GCH4 single element combustion chamber,” Institute for Flight Propulsion (LFA), Technische Universität München, Garching.

[21] E. S. Love, C. E. Grigsby, L. P. Lee and M. J. Woodling, “Experimental and Theoretical Studies of Axisymmetric Free Jets,” NASA, Langley Research Center, 1959.

[22] D. Rist, Dynamik realer Gase, Berlin Heidelberg: Springer-Verlag, 1996.

[23] H. Kuttruff, Acoustics: An Introduction, CRC Press, 2007.

[24] C. Bauer, P. Lungu and O. J. Haidn, “Numerical Investigation of a Resonance Ignition System,” in *8th European Conference for Aeronautics and Space Sciences*, Madrid, 2019.